OPTIMAL BACKSTEPPING CONTROL OF A VR SPHERICAL MOTOR

Kok-Meng Lee and **Raye Sosseh**
Georgia Institute of Technology
George W. Woodruff School of Mechanical Engineering
Atlanta, GA 30332-0405

Abstract

This paper considers the control of a variable reluctance (VR) spherical motor that offers some unique features by combining the roll, pitch and yaw motion in a single joint. The 3-DOF VR motor has multiple independent inputs, and the output torque is direction varying and orientation-dependent and as a result, the control for such a motor is significantly more challenging than the single-axis motor. We formulate a new three-degrees-of-freedom (3-DOF) VR motor control design tool using backstepping, where the inputs are optimized to achieve minimum total energy consumed. The torque has been derived as a linear combination of the square of the input currents, a form computationally friendlier than its quadratic counterpart for real-time implementation. The overall stability of the system is shown using Lyapunov techniques. Simulation results are illustrated to show the performance of the controller.

1. INTRODUCTION

An increasing need for high-performance robotic applications has motivated several researchers to develop new actuators to improve dexterity of robotic wrists. Among these is the ball-joint-like spherical motor (Lee et al., 1996), which combines the roll, pitch and yaw motion in a single joint. The motor operated on the principle of variable reluctance (VR) has a simple structure, no singularities except at its boundary, and the ability to achieve high-positioning precision with fast dynamic response due to its nature of direct drive. These attractive features have potential applications in high-speed wrist motion control, where the orientation must be achieved rapidly and continuously with isotropic resolution in all directions. The trade-off is the need of sophistical control techniques to compensate for the non-linear torque-current characteristics.

In (Lee et al., 1996), the first author and his co-workers presented the dynamic modeling of a 3-DOF VR spherical motor. In this paper, we explore the use of back-stepping control technique to design a stabilizing controller for the spherical motor. The design procedure adopted here has been motivated by and conceptually similar to the framework in utilization of backstepping for solving single–axis VR motor control problems, but we extend it to the 3-DOF actuators. The 3-DOF VR motor has multiple independent inputs, and the output torque is direction varying, and orientation-dependent. These unique features make the control of a 3-DOF VR motor significantly more challenging than the single-axis motor.

This paper offers the following contributions:

1. We formulate a new 3-DOF VR motor control design tool using backstepping, in which the inputs are optimized to achieve minimum total energy consumed. Such formulation enables the utilization of existing adaptive and robust backstepping design techniques for the control of multi-input VR motors; for examples, Carroll and Dawson (1993), Kanellakopoulos (1995), Melkote et al. (1999), and Milman and Bortoff (1999).
2. We present the derivation of the torque model of the 3-DOF VR motor in terms of stator coil inductances, which are given in terms of Euler angles in this paper. In the absence of permanent magnets, the torque is a linear combination of the square of the input currents, a form computationally friendlier than its quadratic counterpart for real-time implementation (Lee et al., 1996).
3. The relationship between the inductance and the air-gap permeance commonly used in the community of stepper motors is also given. The relationship provides an effective means to calculate the stator inductances from the permeance model, which can be computed using finite-element technique, analytically derived using assumed flux-path, or obtained experimentally.

The remainder of this paper is organized as follows: Section 2 models the dynamics of a VR spherical motor appropriate for backstepping design, followed by the design of an optimal backstepping controller in Section 3. In Section 4, we determine the characteristic inductance of the VR motor from the experimentally determined permeance model, verify the assumptions experimentally, and illustrate the backstepping controller with simulation. Finally, conclusions are drawn in Section 5.

2. DYNAMIC MODEL

The assembly of the prototype VR spherical motor is shown in Figure 1. The spherical motor consists of four subassemblies: a rotor, a stator, a bearing system, and a orientation measurement mechanism. The spherical rotor and the hollow spherical stator are concentric and are supported one on the other by means of gimbals. The ferromagnetic poles are strategically distributed on the rotor surface and meet at the center of the rotor. Similarly, the stator poles are distributed on the stator surface, on which the stator coils are wound and can be energized individually. The magnetic conductor layer between the shell and the stator core forms a magnetic circuit with air-gaps connecting the rotor and the stator. The spherical rotor is constrained but allowed to roll

on the bearing gimbals, which are mounted on the inner surface of the stator. The spherical surface of the rotor except for the rotor poles is made up of non-magnetic but hard material.

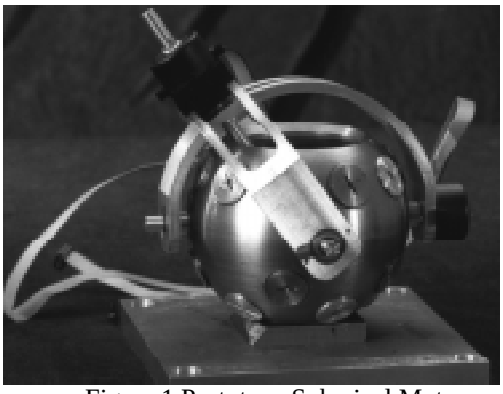

Figure 1 Prototype Spherical Motor

Electromagnetic model

The following assumptions are made in deriving the dynamic model: (1) The reluctance of iron core is negligible as compared to that of the air gap and thus the energy storage solely occurs in the air gap. (2) Leakage flux is assumed to be negligible. (3) The coupling between stator poles may be neglected. (4) The system is electrically linear.

The voltage supply to each coil, $v_i(t)$, must overcome the electrical resistance r and the back electromotive-force (emf) or

$$v_i(t) = u_i(t)r + \frac{d\lambda_i(t)}{dt} \tag{1}$$

where $$\lambda_i = \sum_{j=1}^{M} \lambda_{ij} \qquad i = 1,\ldots,N\ ;\ \ j = 1,\ldots,M\ ; \tag{2}$$

$\lambda_{ij}(t)$ is the flux linkage between i^{th} stator and j^{th} rotor poles; and $u_i(t)$ is the current following through i^{th} stator coil. Since the flux linkage is a function of both current and angular separation between the two interacting poles, its time derivative may be written as follows:

$$\frac{d\lambda_i}{dt} = \frac{\partial\lambda_i}{\partial u_i}\frac{du_i}{dt} + \sum_{j=1}^{M}\frac{\partial\lambda_{ij}}{\partial\varphi_{ij}}\frac{d\varphi_{ij}}{dt} \tag{3}$$

where φ_{ij} is the angle between the position vectors of the i^{th} stator and the j^{th} rotor poles, $\vec{O}_{si}$ and $\vec{O}_{rj}$; and

$$\vec{O}_{rj} = [\mathcal{R}(\psi,\theta,\phi)]\vec{o}_{rj} \tag{4}$$

where $[\mathcal{R}(\psi,\theta,\phi)]$ is a 3x3 rotational matrix describing the rotor orientation with respect to the stator in terms of Z-Y-Z Euler angles; and $\vec{o}_{rj}$ is the position vector of the j^{th} rotor pole in its body-reference-frame. From the dot product of $\vec{O}_{si}$ and $\vec{O}_{rj}$, we have

$$\varphi_{ij}(\psi,\theta,\phi) = \cos^{-1}\left[\frac{\vec{O}_{si}}{R_s}\bullet[\mathcal{R}(\psi,\theta,\phi)]\frac{\vec{o}_{rj}}{R_r}\right] \tag{5}$$

where R_s and R_r are the stator pole-surface from the center of the stator and the rotor radius respectively. Since we have an electrically linear system, i.e.

$$\lambda_{ij} = L_{ij}(\varphi_{ij})\ u_i \tag{6}$$

$$\frac{\partial\lambda_i}{\partial u_i} = \sum_{j=1}^{M} L_{ij}(\varphi_{ij}) = L_i(\psi,\theta,\phi) \tag{7}$$

The quantity $L_i(\psi,\theta,\phi)$ in Equation (7) is referred to as the i^{th} stator inductance. Substituting Equations (3), (6) and (7) into Equation (1), we have

$$v_i(t) = u_i(t)r + L_i(\psi,\theta,\phi)\frac{du_i}{dt} + u_i\frac{dL_i}{dt} \tag{8}$$

Thus, the current dynamics can be represented as

$$\frac{du_i}{dt} = \frac{1}{L_i}\left[v_i - u_i(t)r - u_i(t)\frac{dL_i}{dt}\right] \tag{9}$$

Note that the stator inductance is a function of Euler angles (ψ,θ,ϕ) for a given geometrical. We have

$$\frac{dL_i}{dt} = \frac{\partial L_i}{\partial\psi}\dot{\psi} + \frac{\partial L_i}{\partial\theta}\dot{\theta} + \frac{\partial L_i}{\partial\phi}\dot{\phi} \tag{10}$$

Thus, $$\frac{du_i}{dt} = -\frac{1}{L_i}\left(r + \underline{\ell}_i^T\begin{bmatrix}\dot{\psi}\\ \dot{\theta}\\ \dot{\phi}\end{bmatrix}\right)u_i + \frac{1}{L_i}v_i \tag{11}$$

where $$\underline{\ell}_i^T = \begin{bmatrix}\frac{\partial L_i}{\partial\psi} & \frac{\partial L_i}{\partial\theta} & \frac{\partial L_i}{\partial\phi}\end{bmatrix}. \tag{12}$$

Torque generation

The torque generated by the spherical motor can be derived from the co-energy in the system:

$$\vec{T} = \begin{bmatrix}\frac{\partial W_m}{\partial\psi} & \frac{\partial W_m}{\partial\theta} & \frac{\partial W_m}{\partial\phi}\end{bmatrix}^T \tag{13}$$

where the co-energy,

$$W_m = \sum_{i=1}^{N}\sum_{j=1}^{M}\int_0^{u_j}\lambda_{ij}(\varphi_{ij},u_i)du_i \tag{14}$$

which can be reduced to

$$W_m = \frac{1}{2}\sum_{i=1}^{N} L_i(\psi,\theta,\phi)\ u_i^2 \tag{15}$$

By substituting Equation (15) into Equation (13) and taking the respective partial derivatives, the generated torque is derived in Equation (16),

$$\vec{T} = \begin{bmatrix}T_1\\ T_2\\ T_3\end{bmatrix} = \begin{bmatrix}\underline{\ell}_1 & \cdots & \underline{\ell}_i & \cdots & \underline{\ell}_N\end{bmatrix}\begin{bmatrix}u_1^2\\ \vdots\\ u_N^2\end{bmatrix} \tag{16}$$

which is a function of rotor orientation and the square of the currents applied at the stator coils.

Spherical Motor Dynamics

We define the following state vectors:

$\underline{x}_1 \in \Re^3$ where $\underline{x}_1 = [\psi \quad \theta \quad \phi]^T$; 17(a)

$\underline{x}_2 \in \Re^3$ where $\underline{x}_2 = [\dot{\psi} \quad \dot{\theta} \quad \dot{\phi}]^T$; 17(d)

$\underline{x}_3 \in \Re^N$ where $\underline{x}_3 = [u_1 \quad u_2 \quad \cdots \quad u_N]^T$ 17(c)

and the input vector

$\underline{v} \in \Re^N$ where $\underline{v} = [v_1 \quad v_2 \quad \cdots \quad v_N]^T$. 17(d)

The rotor dynamic equation is given as:

$$\mathbf{M}(\underline{x}_1)\dot{\underline{x}}_2 + \mathbf{h}(\underline{x}_1, \underline{x}_2) = \vec{T} \tag{18}$$

where

$$\mathbf{M}(\underline{x}_1) = \begin{bmatrix} -IS_\theta C_\phi & IS_\phi & 0 \\ IS_\theta S_\phi & IC_\phi & 0 \\ I_z C_\theta & 0 & I_z \end{bmatrix} \tag{18a}$$

$$\mathbf{h}(\underline{x}_1, \underline{x}_2) = \begin{bmatrix} I(-\dot{\psi}\dot{\theta}C_\theta C_\phi + \dot{\psi}\dot{\phi}S_\theta S_\phi + \dot{\theta}\dot{\phi}C_\phi) - (I - I_z)(\dot{\psi}S_\theta S_\phi + \dot{\theta}C_\phi)(\dot{\psi}C_\theta + \dot{\phi}) \\ I(\dot{\psi}\dot{\theta}C_\theta S_\phi + \dot{\psi}\dot{\phi}S_\theta C_\phi + \dot{\theta}\dot{\phi}S_\phi) + (I - I_z)(-\dot{\psi}S_\theta C_\phi + \dot{\theta}S_\phi)(\dot{\psi}C_\theta + \dot{\phi}) \\ -I_z\dot{\psi}\dot{\theta}S_\theta \end{bmatrix} \tag{18b}$$

The spherical motor dynamics can be written as follows:

$$\dot{\underline{x}}_1 = \underline{x}_2 \tag{19a}$$

$$\dot{\underline{x}}_2 = \mathbf{A}(\underline{x}_1, \underline{x}_2) + \mathbf{B}(\underline{x}_1, \underline{x}_2, \underline{x}_3) \tag{19b}$$

$$\dot{\underline{x}}_3 = \mathbf{C}(\underline{x}_1, \underline{x}_2)\underline{x}_3 + \mathbf{D}(\underline{x}_1)\underline{v} \tag{19c}$$

where $$\mathbf{A}(\underline{x}_1, \underline{x}_2) = -\mathbf{M}^{-1}(\underline{x}_1)\mathbf{h}(\underline{x}_1, \underline{x}_2) \tag{19d}$$

$$\mathbf{B}(\underline{x}_1, \underline{x}_2, \underline{x}_3) = \mathbf{M}^{-1}(\underline{x}_1)\begin{bmatrix} \underline{\ell}_1 & \cdots & \underline{\ell}_i & \cdots & \underline{\ell}_N \end{bmatrix}\begin{bmatrix} u_1^2 \\ \vdots \\ u_N^2 \end{bmatrix} \tag{19e}$$

and $\mathbf{C}(\underline{x}_1, \underline{x}_2)$ and $\mathbf{D}(\underline{x}_1)$ are NxN diagonal matrix with their i^{th} row elements respectively given by

$$c_{ii} = -\frac{1}{L_i}\left(r + \underline{\ell}_i^T \underline{x}_2\right); \tag{19f}$$

and $$d_{ii} = \frac{1}{L_i} \tag{19g}$$

3. OPTIMAL BACK-STEPPING CONTROL DESIGN

The dynamic model of the spherical motor has the following cascaded structure:

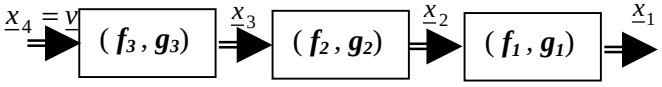

Figure 2 Spherical motor dynamic model

As illustrated in Figure 2, back-stepping design procedure can be applied.

Backstepping

The control variable vector $\underline{v}$ can be used to drive the state $\underline{x}_3$ to any desired state. Similarly, if the state vector $\underline{x}_3$ was the control vector, a stabilizing controller can be designed to drive $\underline{x}_2$ to its desired state. This trend continues with the state $\underline{x}_2$ used to drive $\underline{x}_1$ to follow any desired trajectory. Since $\underline{x}_3$ and $\underline{x}_2$ are not control variables, we define the fictitious control variables $\underline{x}_{3d}$ and $\underline{x}_{2d}$ for a specified trajectory:

$\underline{x}_{1d} \in C^3$, i.e. $\underline{x}_{1d}$, $\dot{\underline{x}}_{1d}$, and $\ddot{\underline{x}}_{1d}$ are available.

We define the following error state vectors:

$\underline{z}_k = \underline{x}_{kd} - \underline{x}_k$; where k=1 , 2, and 3 (20)

where $\underline{x}_{2d}$ and $\underline{x}_{3d}$ are virtual controls to be defined. The fictitious controllers for the subsystems are chosen such that

$$\dot{\underline{z}}_k = -\alpha_k \underline{z}_k, \quad \text{where } \alpha_k > 0 \tag{21}$$

$$\Rightarrow \underline{z}_k = 0 \text{ asymptotically}$$

Equation (20) defines the error between the desired and the actual states. The choice of two fictitious and the actual control inputs ($\underline{x}_{3d}$, $\underline{x}_{2d}$, and $\underline{v}$) defined by Equation (22) ensures that z_k will converge to zero and thus guarantees the asymptotic stability of z_k:

$$\mathbf{g}_1(\underline{x}_1, \underline{x}_{2d}) = \alpha_1 \underline{z}_1 + \dot{\underline{x}}_{1d} - \boldsymbol{f}_1(\underline{x}_1) \tag{22a}$$

$$\mathbf{g}_2(\underline{x}_1, \underline{x}_2, \underline{x}_{3d}) = \alpha_2 \underline{z}_2 + \dot{\underline{x}}_{2d} - \boldsymbol{f}_2(\underline{x}_1, \underline{x}_2) \tag{22b}$$

$$\mathbf{g}_3(\underline{x}_1, \underline{x}_2, \underline{x}_3, \underline{v}) = \alpha_3 \underline{z}_3 + \dot{\underline{x}}_{3d} - \boldsymbol{f}_3(\underline{x}_1, \underline{x}_2, \underline{x}_3) \tag{22c}$$

Optimal controller design for the VR spherical motor

In designing the controller, the electrical dynamics are neglected. This is justified by our use if analog current amplifiers, which serve to compensate the electrical dynamics with high gain feedback, increasing the electrical subsystem, Equation (19c) and the mechanical subsystem, Equations (19a) and (19b).

Since $\boldsymbol{f}_1(\underline{x}_1) = 0$ and $\boldsymbol{g}_1(\underline{x}_1, \underline{x}_2) = \underline{x}_2$, we have the fictitious controller from Equation (22a),

$$\underline{x}_{2d} = \alpha_1(\underline{x}_{1d} - \underline{x}_1) + \dot{\underline{x}}_{1d} \tag{23}$$

where $\underline{x}_{1d}$ and $\dot{\underline{x}}_{1d}$ are the desired rotor orientation and its 1^{st} time derivative. Note that the choice of $\underline{x}_{3d}$ requires the time derivative of $\underline{x}_{2d}$, which is given by

$$\dot{\underline{x}}_{2d} = \alpha_1(\dot{\underline{x}}_{1d} - \underline{x}_2) + \ddot{\underline{x}}_{1d} \quad (24)$$

Substituting Equations (23) and (24) into Equation (22b), we have

$$\mathbf{g}_2(\underline{x}_1, \underline{x}_2, \underline{x}_{3d}) = \begin{bmatrix}\alpha_1\alpha_2 & \alpha_1+\alpha_2 & 1\end{bmatrix}\begin{bmatrix}\underline{x}_{1d}-\underline{x}_1 \\ \dot{\underline{x}}_{1d}-\underline{x}_2 \\ \ddot{\underline{x}}_{1d}\end{bmatrix} - \boldsymbol{f}_2(\underline{x}_1, \underline{x}_2) \quad (25)$$

However, $\mathbf{g}_2(\underline{x}_1, \underline{x}_2, \underline{x}_{3d})$ implicitly contains the generated motor torque vector $\vec{T}$ that is a function of the square of the currents. The fictitious current control $\underline{x}_{3d}$, the desired trajectory for the current state $\underline{x}_3$, is solved in two steps:

The *first* step determines the desired torque needed to drive the rotor to the desired orientation, which can be obtained from equation (25):

$$\vec{T}_d = \mathbf{M}(\underline{x}_1)\left[\alpha_1\alpha_2\underline{z}_1 + (\alpha_1+\alpha_2)\dot{\underline{z}}_1 + \ddot{\underline{x}}_{1d}\right] + \boldsymbol{h}(x_1, x_2) \quad (26)$$

The *second* step is to solve for $\underline{x}_{3d}$, which is formulated as a minimization of the total energy

$$J = \frac{1}{2}\underline{x}_3^T\underline{x}_3 \quad (27)$$

subjected to the constraint imposed by Equation (16) with $\vec{T} = \vec{T}_d$ and $0 \le u_i^2 \le u_{\max}^2$. Note that the number of stator poles is greater than the DOF (N > 3) and the three rows of $\begin{bmatrix}\underline{\ell}_1 & \cdots & \underline{\ell}_i & \cdots & \underline{\ell}_N\end{bmatrix}$ are linearly independent,

$$\text{Rank}\begin{bmatrix}\underline{\ell}_1 & \cdots & \underline{\ell}_i & \cdots & \underline{\ell}_N\end{bmatrix} = 3.$$

From the fundamental theorem of linear programming, the existences of basic feasible solutions to the constraint equations ensure the existence of the optimal solution to the above problem. Therefore, with the desired current found, the overall system is asymptotically stable. The stability argument can also be verified using Lyapunov stability analysis as follows. With a Lyapunov function

$$V = \alpha_1\underline{z}_1^T\underline{z}_1 + \alpha_2\underline{z}_2^T\underline{z}_2 \quad (28)$$

the solution to the linear programming problem yields exponential stability as

$$\dot{V} = 2\left(\alpha_1\underline{z}_1^T\dot{\underline{z}}_1 + \alpha_2\underline{z}_2^T\dot{\underline{z}}_2\right)$$

which implies

$$\dot{V} = -2\left(\alpha_1^2\underline{z}_1^T\underline{z}_1 + \alpha_2^2\underline{z}_2^T\underline{z}_2\right) < 0 \quad (29)$$

4. EXPERIMENTAL AND SIMULATION RESULTS

Figure 3 is an equivalent circuit of the spherical motor. In Figure 3, R_{ij} is the reluctance of the air-gap between the i^{th} stator and j^{th} rotor poles. The 5 rotor poles are arranged at the apices of an octahedron with the topmost pole removed to provide an area for attaching the output shaft. The 10 stator-poles are placed on the apices of an icosahedron without the topmost and bottommost poles.

Relationship between stator inductance and permeance

The permeance P that is a reciprocal of the reluctance has been determined experimentally (Lee *et al*., 1996) as a function of the angular displacement between an adjacent pair of stator/rotor poles for the prototype spherical motor.

$$P(\varphi) = \begin{cases} a_0 & \varphi > 1.2417 \\ \sum_{i=0}^{6} a_i\varphi^i & \varphi \le 1.2417 \end{cases} \quad (30)$$

where φ is the angular displacement between a pair of rotor and stator poles; and

a_0 = 6.1553E-07 a_1 =6.5365E-08 a_2 = -3.7298E-06
a_3 = 6.1471E-06 a_4 = -3.9278E-06 a_5= 7.7800E-07
a_6 = 8.4387E-08 a_7 = 5.3668E-08

Since the flux linkage is defined as

$$\lambda_{ij} = n\Phi_{ij} \text{ where } \Phi_{ij} = \frac{nu_i}{R_{ij}} = nu_iP_{ij}; \quad (31)$$

n is the number of turns in each of the stator coils; Φ_{ij} is the flux flowing through the air-gap between the i^{th} stator and j^{th} rotor poles. Substituting λ_{ij} Equation (6) into Equation (31), which leads to

$$L_{ij} = n^2P_{ij}$$

and using Equation (2) and (7), we have

$$L_i(\psi, \theta, \phi) = n^2\sum_{j=1}^{M} P(\varphi = \varphi_{ij}) \quad (32)$$

Figure 4 shows a typical inductance in terms of Euler angles.

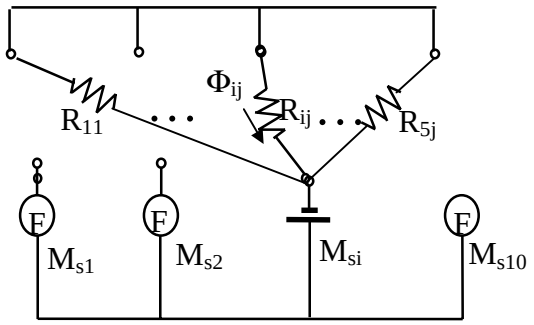

Figure 3 Equivalent circuit of the spherical motor

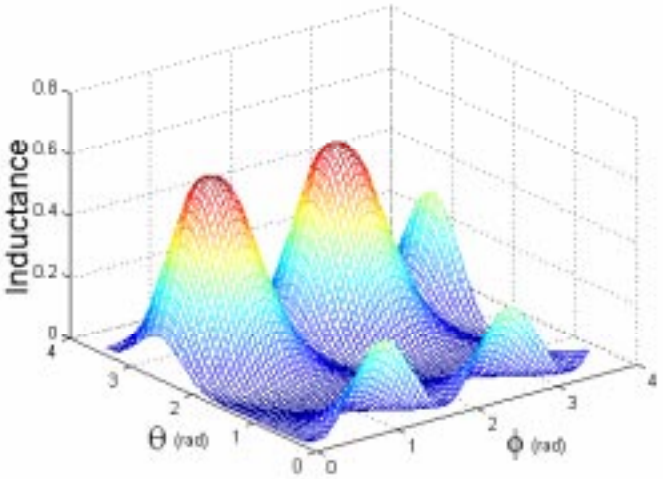

Figure 4 Inductance (ψ=0.75 radians)

Linearity and mutual inductance

In investigating the extent to the coupling effect and linearity of the inductances in the spherical motor, a stator pole was excited with a step current. The voltage responses of the excited stator as well as the adjacent stator coils were recorded. For a locked rotor, the inductances are constant. For a step change in current, the voltage across the excited coil would be a combination of an impulse (as a result of the derivative of the current) and a steady-state voltage across the coil resistance as illustrated in Equation (8), and that across each of the unexcited coils would be due primarily to mutual inductance. As shown in Figure 5, the voltage response in the excited stator coil #1 was significantly larger than the adjacent stator poles #2 and #5. Thus, the contribution of the flux linkage due to the induced current is negligible.

The flux linkage can be determined experimentally As illustrated in Equation (1):

$$\lambda_i = \int_0^t [v_i(t) - u_i(t)r]dt$$

Figure 6 shows that the flux linkage integrated over the voltage difference for several values of a step current input. The result shows that the inductance is linear with current excitation to about 1 ampere, beyond which the flux linkage saturates and the inductance decrease with further increase in current input.

Simulation results

Figure 7 compares the desired and output rotor trajectory in terms of Euler angles and the corresponding output torque. Good orientation tracking performance is obtained as may be seen from Figure 7. The optimized currents are given in Figure 8. With a few exceptions, most of the input currents needed were within 2 amperes for the period of 5 seconds.

5. CONCLUSIONS

A new 3-DOF VR motor control design using backstepping has been presented, where the inputs are optimized to achieve minimum total energy consumed. It is expected that this design provides an essential basis for the control of multi-input VR motors utilizing backstepping.

We derive the torque model in terms of stator inductances, a form more appropriate for backstepping design of a 3-DOF VR spherical motor. It has been shown that in the absence of permanent magnets, the torque is a linear combination of the square of the input currents, which is computationally friendlier than its quadratic counterpart. Such a formulation enables the utilization of existing adaptive and robust backstepping for the control of 3-DOF VR motors.

The relationship between the inductance and the air-gap permeance is also given, which has been used to calculate the stator inductances from the experimentally permeance model. Finally, the overall stability of the system is shown using Lyapunov techniques. Simulation results have illustrated the performance of the controller.

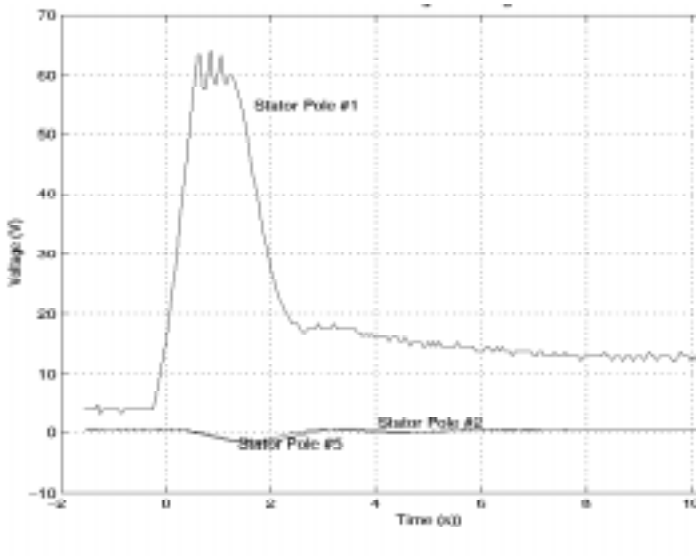

Figure 5 Coupling effect

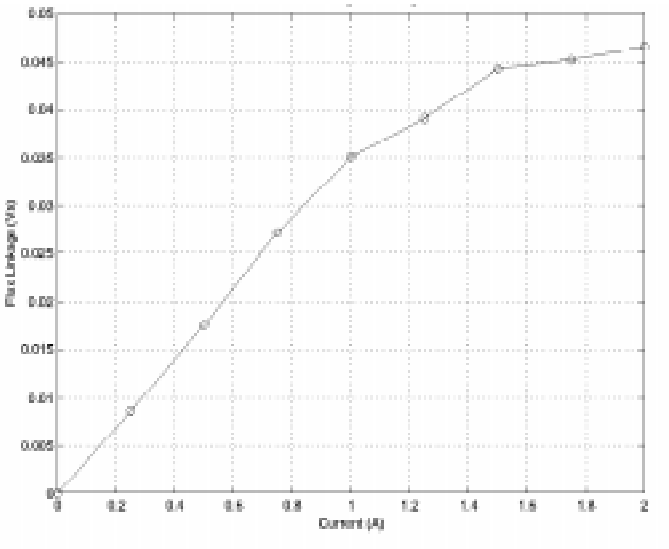

Figure 6 Linearity

REFERENCE

Carroll, J. and D. Dawson, (1993), "Adaptive Tracking Control of a switched Reluctance Motor Turning an Inertia Load," *Proc. ACC*, San Francisco, CA, June, pp. 670-674.

Kanellakopoulos, I., (1995) "Block Backsteeping for Adaptive Nonlinear Control," IFAC Nonlinear Control Systems Design, Tahoe City, CA.

Lee, K.-M., R. Roth, and Z. Zhou, (1996) "Dynamic Modeling and Control of a Ball-Joint-Like VR Spherical Motor," *ASME J. Dyn. Sys, Meas, and Control*, Vol. 118, No. 1, March, pp.29-40.

Melkote, H., F. F. Khorrami, S. Jain, and M. S. Mattice, (1999) "Robust Adaptive Control of Variable Reluctance Motors," IEEE Trans. Control Sys. Tech., Vol. 7, No. 2 March, pp.212-221.

Milman R. and S, A. Bortoff, (1999), Observer-based Adaptive Control of a Variable Reluctance Motor: Experimental Results," IEEE Trans. Control Sys. Tech., Vol. 7, No. 5 March, pp. 613-621.

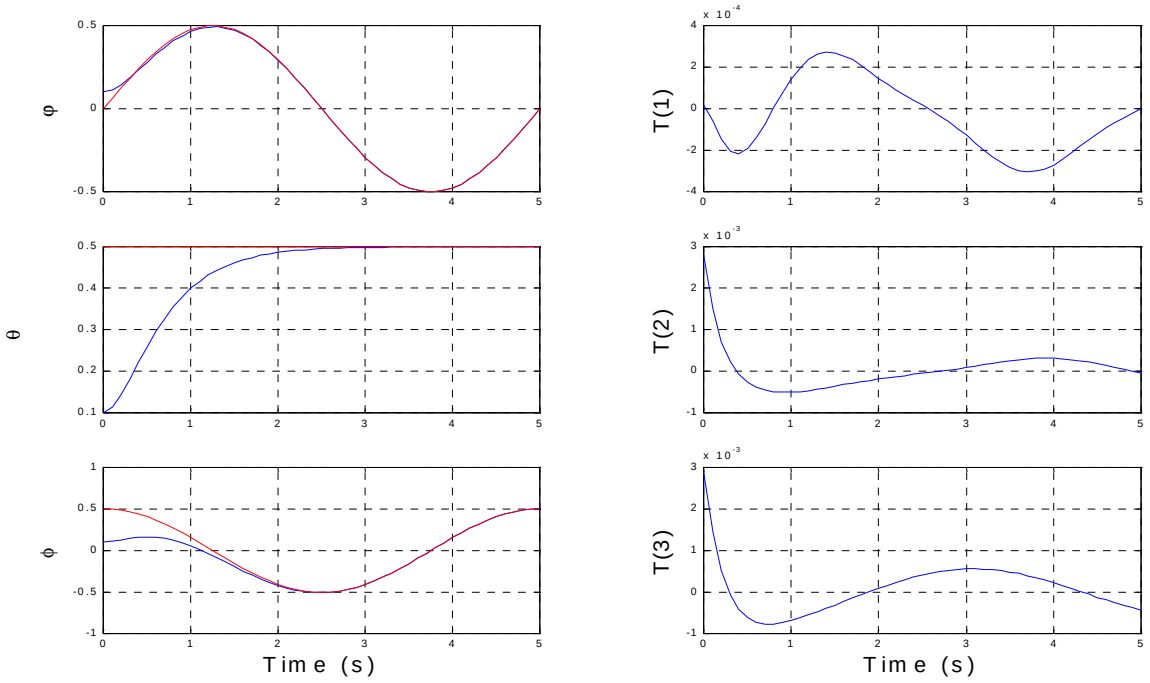

Figure 7 Trajectory and torques

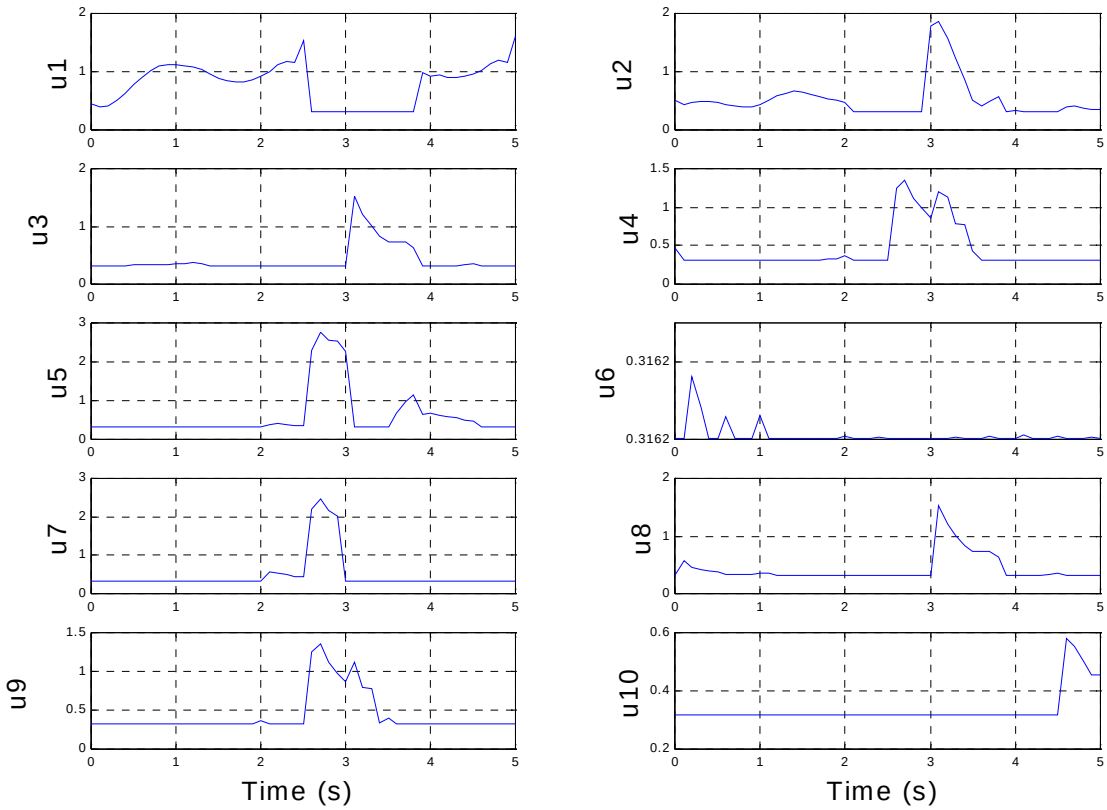

Figure 8 Input currents